HHS Public Access

Author manuscript

J Neurosci Res. Author manuscript; available in PMC 2023 April 01.

Published in final edited form as:

J Neurosci Res. 2023 April ; 101(4): 464–479. doi:10.1002/jnr.25158.

Peptidyl arginine deiminase 4 deficiency protects against subretinal fibrosis by inhibiting Müller glial hypercitrullination

Sarah I. Palko,

Nicholas J. Saba,

Paola Bargagna-Mohan,

Royce Mohan

Department of Neuroscience, University of Connecticut Health Center, Farmington, Connecticut, USA

Abstract

Retinal scarring with vision loss continues to be an enigma in individuals with advanced age-related macular degeneration (AMD). Müller glial cells are believed to initiate and perpetuate scarring in retinal degeneration as these glial cells participate in reactive gliosis and undergo hypertrophy. We previously showed in the murine laser-induced model of choroidal neovascularization that models wet-AMD that glial fibrillary acidic protein (GFAP) expression, an early marker of reactive gliosis, increases along with its posttranslational modification citrullination. This was related to increased co-expression of the citrullination enzyme peptidyl arginine deiminase-4 (PAD4), which also colocalizes to GFAP filaments. However, whether such hypercitrullination in Müller glial drives fibrotic pathology has remained understudied. Here, using male and female C57Bl6 mice subjected to laser injury, we investigated in a temporal study how citrullination impacts GFAP and PAD4 dynamics. We found that high molecular weight citrullinated species that accumulate in Müller glia corresponded with dynamic changes in GFAP and PAD4 showing their temporal redistribution from polymeric cytoskeletal to soluble protein fractions using immunostaining and western blot analysis. In conditional glial-specific PAD4 knockout (PAD4cKO) mice subjected to laser injury, there was a stark reduction of citrullination and of polymerized GFAP filaments. These injured PAD4cKO retinas showed improved lesion

Correspondence: Royce Mohan, Department of Neuroscience, University of Connecticut Health Center, 263 Farmington Avenue, Farmington, CT 06030, USA. mohan@uchc.edu.

AUTHOR CONTRIBUTIONS

All authors had full access to all the data in the study and take responsibility for the integrity of the data and the accuracy of the data analysis. *Conceptualization*, P.B.-M. and R.M.; *Methodology*, S.I.P., N.J.S., P.B.-M., and R.M.; *Investigation*, S.I.P., N.J.S., P.B.-M., and R.M.; *Formal Analysis*, S.I.P., P.B.-M., and R.M.; *Resources*, R.M.; *Writing – Original Draft*, S.I.P. and R.M.; *Writing – Review & Editing*, S.I.P., N.J.S., P.B.-M., and R.M.; *Visualization*, S.I.P., P.B.-M., and R.M.; *Supervision*, R.M. and P.B.-M.; *Funding Acquisition*, R.M.

DECLARATION OF TRANSPARENCY

The authors, reviewers and editors affirm that in accordance to the policies set by the *Journal of Neuroscience Research*, this manuscript presents an accurate and transparent account of the study being reported and that all critical details describing the methods and results are present.

SUPPORTING INFORMATION

Additional supporting information can be found online in the Supporting Information section at the end of this article.

CONFLICT OF INTEREST

The authors declare that the research was conducted in the absence of any commercial or financial relationships that could be construed as a potential conflict of interest.

healing, as well as reduced fibronectin deposition in the subretinal space at 30 days. Taken together, these findings reveal that pathologically overexpressed PAD4 in reactive Müller glia governs GFAP filament dynamics and alters their stability, suggesting chronic PAD4-driven hypercitrullination may be a target for retinal fibrosis.

Keywords

citrullination; GFAP; Müller glial endfeet; PAD4; retinal gliosis; RRID:AB_2338508; RRID:AB_2534091; RRID:AB_2535713; RRID:AB_2535813; RRID:AB_2572090; RRID:AB_2762843; RRID:AB_2802127; RRID:AB_304558; RRID:AB_306067; RRID:AB_650499; RRID:AB_650500; RRID:AB_881875; RRID:IMSR_JAX:012849; RRID:IMSR_JAX:026708; RRID:SCR_002798; RRID:SCR_003070; subretinal fibrosis

1 | INTRODUCTION

Age-related macular degeneration (AMD) is the leading cause of vision loss for the aging population in developed nations (Ambati et al., 2003). This retinal disease is characterized by degeneration of the macula, the densely populated area of cone photoreceptors that provides central vision and acuity. AMD has two distinct forms—dry and wet—both affecting the photoreceptors in the macula. Dry-AMD evokes gradual vision loss, and accumulation of lipid deposits called drusen below the retinal pigment epithelium (RPE). In contrast, wet-AMD occurs when choroid blood vessels penetrate the Bruch's membrane, damaging the RPE and photoreceptors, resulting in vascular leakage. Whereas dry-AMD is more prominent, wet-AMD progresses faster and causes acute loss of vision due to choroidal neovascularization (CNV). Despite available treatments that target CNV, many wet-AMD patients develop scarring and permanent vision loss. One key player in the perpetuation of scarring in AMD may be glial cells, as they contribute to scarring via chronic gliosis (Telegina et al., 2018).

Retinal gliosis is a reactive process driven mainly by Müller cells, the predominant glial cell type in the retina (Bringmann et al., 2009). Müller cells are responsible for trophic support of the photoreceptors and retinal neurons and they become reactive, proliferative, and hypertrophic upon injury or insult. While gliosis can be neuroprotective in response to acute injury, its sustained activation causes pathologies associated with a wide range of neurodegenerative retinal diseases, including AMD (Wu et al., 2003).

The hallmark of gliosis is increased expression of the intermediate filament (IF) proteins glial fibrillary acidic protein (GFAP) and vimentin in Müller cells (Bringmann & Wiedemann, 2012). In the retina, overabundance of IF proteins can cause mechanical distortion, and cell death (Edwards et al., 2017; Verardo et al., 2008). Mice lacking both GFAP and vimentin showed reduced photoreceptor damage after retinal detachment, indicating that these two IF proteins play a significant role in the perpetuation of glial scarring (Verardo et al., 2008). Moreover, targeting the chronic overexpression of either IF protein in adult mice to overcome embryonic compensatory mechanisms have revealed that GFAP and vimentin contribute to MG hypertrophy in a retinal disease model (Hippert et al., 2021). Upon insult or injury, GFAP and vimentin undergo posttranslational

modifications (PTMs) such as phosphorylation, which play important roles in altering their IF structures and abundance of soluble IF precursors, and consequentially, govern cell behaviors (Eriksson et al., 2004; Hol & Capetanaki, 2017; van Bodegraven & Etienne-Manneville, 2021). One notable PTM affecting IF proteins, but is relatively understudied, is citrullination (Briot et al., 2020). Citrullination is an irreversible modification of protein arginine residues by the α-amino acid citrulline, an enzymatic reaction catalyzed by peptidyl arginine deiminases (PADs) (Witalison et al., 2015).

Citrullinated proteins have been recognized as biomarkers in several major autoimmune and chronic fibrotic diseases and targeting PADs has shown benefits in several preclinical models (Lewis et al., 2015; Nicholas et al., 2004; Willis et al., 2017). Notably, it was shown that citrullination is increased in human wet-AMD eyes, but PAD2 levels were not (Bonilha et al., 2013), suggesting that other PADs may be responsible for disease-related citrullination in the retina (Hollingsworth et al., 2018). Among the five PADs, PAD2 and PAD4 are expressed in normal murine retinas, while PAD4 gene and protein expression was shown to be induced in retinas following ocular exposure to alkali (Wizeman et al., 2016; Wizeman & Mohan, 2017). These findings suggested that PAD4 may play a key role in citrullination during Müller cell gliosis.

Citrullination of GFAP filaments occurs very early after injury, and PAD4 colocalization on these filaments occurs concomitantly in reactive Müller glia (Wizeman et al., 2016; Wizeman & Mohan, 2017). PAD4 colocalization on filamentous GFAP was also observed in the murine laser-induced model of CNV (Palko et al., 2022). Defining PAD4's key role in this PTM, conditional glial-specific PAD4 knockout (PAD4cKO) mice subjected to laser injury showed significantly reduced hypercitrullination (Palko et al., 2022). However, whether such a mechanism occurs in genetic diseases was subsequently revealed in a genetic model of spontaneous retinal degeneration (JR5558 mice) that revealed heightened citrullination (hypercitrullination), with both citrullinated GFAP and PAD4 being localized in reactive Müller glia. Such maladaptive chronic retinal hypercitrullination was also seen in severely diseased human wet-AMD maculae demonstrating that hypercitrullination is retained into end stages of retinal disease (Palko et al., 2022). Because Müller glial endfeet play such a critical role in pathological hypercitrullination, we have termed it the citrullination bunker (Palko et al., 2022).

In this study, we examined the PAD4-citrullination axis to study how reactive gliosis contributes to subretinal fibrosis (Ishikawa et al., 2016) and focused on citrullination of GFAP, as this IF protein serves an internal reference for the global citrullination changes occurring in reactive Müller glia. Through use of the PAD4cKO mice in experimental laser-induced retinal gliosis we demonstrate an important role for PAD4 in pathological hypercitrullination and suggest that PAD4 may also be an important target for subretinal fibrosis.

2 | METHODS AND MATERIALS

2.1 | Mice and laser injury

C57BL/6J mice were purchased from the Jackson Laboratory (Bar Harbor, ME), and maintained in-house. The laser injury model of CNV (Liu et al., 2019) was used as an experimental means to elicit and study acute and chronic retinal gliosis (Palko et al., 2022), adopting this model to examine subretinal fibrosis (Ishikawa et al., 2016). Equal numbers of male and female mice, at 3 to 5 months of age were used as done previously (Palko et al., 2022). In brief, mice were anesthetized using an intraperitoneal injection of ketamine/xylazine according to body weight and phenylephrine and tropicamide were applied topically to dilate pupils. GenTeal eye gel (Alcon Laboratories, Inc.) was applied on the cornea to facilitate contact with the microscope lens. Mice were placed on a holder in front of the imaging objective of the Micron III Imaging System (Phoenix, AZ). The objective lens was advanced to contact the mouse cornea and the retinal pigment epithelium (RPE) was brought into focus. The Meridian Merilas Nd-Yag 532 nm alpha green laser photocoagulator integrated with the Micron III camera was employed to produce the laser burns on the RPE. First, a low power red laser was employed to guide the position of laser spot on the retina prior to use of the green laser for tissue ablation. The 532 nm laser beam of 50 μm in diameter was employed to deliver 250 mW at 100 ms focal lesions in six to eight equally spaced regions in a circular pattern surrounding the optic nerve. This laser injury protocol was optimized to produce reproducible retinal lesions marked by chronic gliosis that resulted in subretinal fibrosis. Care was taken to avoid targeting tissue close to retinal blood vessels. Mice were recovered on heating pads and transferred to standard cages upon recovery. Upon euthanasia, mouse eyes were enucleated, immediately frozen on dry ice, and maintained at −80°C. Mice were euthanized at three time points: 7-, 16-, and 30-days post-laser injury.

Male and female B6.Cg-Tg(GFAP-cre/ERT2)505Fmv/J (Stock No: 012849; Jackson Laboratory, Maine; termed GFAP-CreERT2 in short; RRID:IMSR_JAX:026708) mice were purchased and breeding colonies established. We also purchased B6.Cg-Padi4tm1.2Kmow/J (Stock No: 026708; Jackson Laboratory, Maine; termed Padi4flox/flox in short; RRID:IMSR_JAX:012849) male and female mice and bred this line in-house at the Center for Mouse Genome Modification. Colonies of both transgenic lines were maintained as breeders. The GFAP-CreERT2 line was crossed with Padi4flox/flox line through a breeding strategy (Scheme 1) to obtain the desired double-transgenic PAD4cKO mouse line. This procedure involved selecting the correct genotype of the mouse pups using polymerase chain reaction and maintaining them to adulthood for subsequent breeding experiments. Once all founder breeding lines were established, subsequent mouse breeding was done to obtain a large enough colony size of each line for use in experiments. Starting 1 day prior to laser injury, adult male and female PAD4cKO and transgenic Padi4flox/flox mice (termed control) were administered tamoxifen for 4 days by intraperitoneal (i.p.) injection to induce Cre expression (see Scheme 2) in reactive glial cells as previously reported (Palko et al., 2022). Following this protocol, we found a 5.9-fold reduction of PAD4 protein levels in PAD4cKO compared to the control injured mice providing evidence of sufficient PAD4

target deficiency (Palko et al., 2022). Tamoxifen-injected mice were placed in vented cages and housed in a dedicated chemical isolation room until analyzed.

2.2 | Western blot analysis

Mice were euthanized and enucleated 7 and 16 days after laser injury for these experiments. The anterior ocular tissues were carefully separated from the posterior eye cups and the latter tissue (collected from a pool of 2 eyes) was employed for protein extraction. We performed separate extractions for each of the western blot analysis. Tissues were minced in ice-cold soluble buffer (20 mM Tris buffer, 200 mM NaCl, 1% NP-40, 1 mM sodium vanadate, and 1 mM phenylmethyl sulfonyl fluoride) supplemented with a proteinase inhibitor cocktail (Roche, Indianapolis, IN), as previously described (Wizeman et al., 2016). Samples were left on ice for 45 min and then spun at 14,000× *g* for 5 min at 4°C. The supernatant was removed, sheared through the tip of a p200 pipette, and spun again at 14,000× *g* for 5 min. The supernatants representing the "soluble fractions" were collected and kept on ice. The protein concentration of the soluble fractions was quantified using a BSA standard curve and a BCA kit (Pierce BCA Assay), and typically 20 µg protein was loaded. The insoluble pellets were extracted with 2× ß-mercaptoethanol/Laemmli buffer, frozen/thawed (dry ice/warm water), and vortexed for 30 s, repeating this process three times. These extracts representing the cytoskeletal (insoluble) fractions were centrifuged at 14,000× *g* for 5 min at room temperature to pellet debris. The supernatants were used as the cytoskeletal fraction, which we previously estimated to contain 12 microgram protein (Wizeman et al., 2016; Wizeman & Mohan, 2017). Soluble and cytoskeletal fractions were finally boiled at 100°C for 10 min, and soluble and cytoskeletal fractions were separately analyzed by western blotting.

Protein was run on Criterion TGX Stain-Free 4%–20% gels (BIO-RAD, CA). These stain-free gels were imaged on a BioRad gel dock imager (ChemiDoc XRS+ Gel Imaging System, BIO-RAD, CA) and subsequently transferred onto nitrocellulose membranes as described (Palko et al., 2022). Chemiluminescence was used to visualize western blot bands on the BioRad gel dock imager, and images of stain-free blot loading were used as a loading control for all western blot analysis as done previously (Palko et al., 2022) following other published literature (Rivero-Gutierrez et al., 2014). This method of normalization offers a more linear range and decreased variability compared to common housekeeping genes (Rivero-Gutierrez et al., 2014). ImageJ (also known as FIJI) software (RRID:SCR_003070) was used to measure density of bands and the arbitrary units were calculated by dividing the density reading of the target protein band on western blots divided by the stain-free density reading for that respective sample lane (between 37 kDa and top of gel). Quantitation and statistical analysis of data was performed using GraphPad PRISM statistical software (see Statistical Analysis).

2.3 | Immunostaining

Mice were euthanized and eyes enucleated 7, 16, and 30 days after laser injury for these experiments. Mouse eyes from control and injured eyes were enucleated, immediately embedded in optimum cutting temperature compound (OCT; Tissue-Tek, Radnor, PA), and stored at −80°C. Immunostaining was performed as previously described (Palko et

al., 2022; Wizeman et al., 2016). Briefly, 12 μm cryo-sections were air dried for 30 min at room temperature, fixed with 4% paraformaldehyde/PBS for 10 min, and then washed three times for 5 min with PBS. Samples were probed with primary antibodies (Table 1) diluted in DAKO background reducing solution (Agilent, S3022) at 37°C for 3 h or overnight at 4°C. After three washes with PBS for 15 min, slides were then incubated with secondary antibodies (Table 1) for 1 h at room temperature (RT), and then washed three times for 10 min before imaging. Stained sections were routinely imaged using an Olympus IX81 epifluorescence microscope with 20× objective and MetaMorph software to ascertain staining efficiency. Some higher magnified images were captured employing 40× objective on a Leica THUNDER 3D imager microscope with Leica software. Immunofluorescence images were quantified using ImageJ software. The immunostained area of protein expression in lesions was quantified and compared between control and laser injured groups. Three different sections from each mouse were considered in quantification studies. This analysis method was also used for the knockout mouse studies, and area of staining in the lesions was quantified and compared between control laser injured and PAD4cKO laser injured groups.

2.4 | Quantification of lesion size and antibody staining from retinal sections

For fundus imaging, mice were anesthetized and both eyes were lasered as described (Section 2.1). Fundus images were obtained at 30 days post-injury using the Micron III fundus camera. Images of lesions were collected, and a random set from those with clear visualization of lesions were used for quantification (52 lesions from 7 control mice and 76 lesions from 10 PAD4cKO mice randomized to sample both left and right eyes in each group). Lesion size was measured following the instructions in ImageJ software (https://imagej.nih.gov/ij/docs/menus/analyze.html#ap). The retinal fundus image was opened from within the application and converted to gray scale 8-bit image. Next, individual lesions were selected, and each processed separately. First, the rectangle drawing tool in ImageJ was used to demarcate a square border around the lesion. From the Image menu the dropdown Duplicate menu was selected and applied that resulted in a new smaller window appearing containing only the selected lesion image. This lesion image was subjected to thresholding by selecting from Image menu → Adjust from the dropdown and then → Threshold. The lesion area appeared red against the gray background. To reduce background, the brightness and contrast was adjusted. This allowed the circular lesion represented by the red color to be clearly defined, which was converted to binary image after thresholding. From the Analyze menu the dropdown Analyze Particles was then selected. This produces a new window with a dialog box that was configured (Size: 0-infinity; Circularity: 0.00–1.00; Show: Outlines). By additionally selecting Display results and Summarize in this menu the area of the stained region was reported. This process was repeated for individual lesions for all the samples. Quantitation and statistical analysis of data was performed using GraphPad PRISM statistical software (see Statistical Analysis). For the immunostained retinal images, we employed a similar method for analysis. The fluorescent image was opened from within the application and converted to a gray scale 8-bit image (see File S2). Next, the rectangle drawing tool was used to demarcate a fixed size rectangular border that encompassed the entire stained region of interest (GCL to RPE) for GFAP, PAD4, and F95 staining. The subretinal region was demarcated for fibronectin staining. From the Image

menu the dropdown Duplicate was selected and when applied resulted in a new smaller window containing the selected rectangular region to appear. This image was subjected to thresholding by selecting from Image menu → Adjust from the dropdown and then → Threshold. The stained areas first appeared red against the black background and upon thresholding they became binary images. These binary images were analyzed as done above.

2.5 | Rigor and reproducibility

Two separate individuals performed quantification separately to achieve unbiased measurements. Samples were randomized by arbitrarily selecting either left or right eyes from within each group. To randomize the analysis, different batches of C57BL/6 mice procured from the vendor were subjected to experimental injury over a 2-year period. The uninjured mice also came from these batches and were randomly selected. Laser injury experiments on the male and female PAD4cKO mice and control transgenic mice were also performed on different cohorts of animals that were bred for over 2 years from different founder lines. Three trained individuals performed the laser injuries at different times in this study, and as such, eyes from such separate experiments were collectively used for analysis. Mice of both sexes were employed, and the sex of mice were recorded, although the analyses were performed blinded to the sex. As no significant differences were noted in the results after revealing of the sex, these findings represent responses of male and female mice to the laser injury.

2.6 | Statistical analysis

Statistical analysis was performed using GraphPad Prism 9 software (Graph Pad Software, San Diego, CA, USA; RRID:SCR_002798). Experiments were designed for sample size of $N = 10$ mice/group based on our prior studies that tested for significant differences in these same protein targets investigating injury-related retinal gliosis (Wizeman et al., 2016; Wizeman & Mohan, 2017). These targets have also been investigated in the optimized laser injury protocol to study retinal gliosis (Palko et al., 2022) that was employed here. Routine experiments were typically conducted using $N = 4–5$ mice/group and entire experiments were repeated over different days to attain the sample size. On infrequent occasions, if the laser burn caused retinal microvascular hemorrhage to occur then those mice were excluded from analysis. Such technical issues and loss of blots to background issues preventing analysis resulted in fewer samples for some analysis than what was planned originally. Western blot data were analyzed using the Kruskal-Wallis nonparametric test with Dunn's multiple comparisons using statistical hypothesis testing as values did not show a normal distribution. The H statistic is reported. Groups were considered independent and comparisons of the 7- and 16-day injury samples to the control group was made as unpaired samples. A value of $p < .05$ was considered significant. For the data derived from analysis of immunostained retinas and fundus lesion which did not show a normal distribution the Mann–Whitney two-tailed nonparametric test was employed, and samples were considered independent. The U statistic is reported. For analysis of immunostained retinal data that showed normal distribution the two-tailed unpaired parametric t test with Welch's correction without assuming equal standard deviation (SD) was employed. The t statistics is reported. A value of $p < .05$ was considered significant.

3 | RESULTS

3.1 | Citrullination is localized to GFAP filaments in laser-induced retinal gliosis

We recently established that polymeric, citrullinated GFAP is detectable in endfeet of reactive Müller glia in the laser-injury mouse model of CNV. These findings revealed that activation of citrullination in Müller glia is lesion specific (Palko et al., 2022). Here, we extended this study to determine the temporal regulation of citrullination during laser injury-induced retinal gliosis by first examining retinal tissue at 7 days post-laser injury (Fabian-Jessing et al., 2022). This time point reflects the growth and remodeling of GFAP filaments in reactive Müller glia whose cell processes span the thickness of the retina extending to the fibrovascular lesion (Giani et al., 2011; Ishikawa et al., 2016) paralleling similar IF protein dynamics as observed in the alkali injury model (Wizeman et al., 2016). As anticipated, in uninjured retinas, GFAP was mainly localized to ganglion cell layer (GCL) astrocytes (Bargagna-Mohan et al., 2010), whereas in 7-day injured retinas, GFAP was localized in Müller cells from the endfeet through all layers of the retina, terminating at the level of the degenerated photoreceptor outer segments marking the lesion site (Figure 1).

Citrullination (F95 staining) was confined to retinal blood vessels in control retinas but was observed in long Müller cell processes colocalizing with GFAP staining in injured retinas (Figure 1). The staining of GFAP and F95 was quantified (see Methods and File S2) and both proteins showed a significant increase in the lesion site compared to uninjured retinas (Figure 1b). This pattern of staining is consistent with previous findings showing citrullination colocalizes with GFAP as revealed by confocal microscopy (Palko et al., 2022), but also identifies that GFAP is modified in injured retinas in a manner similar to that found in alkali injury (Wizeman et al., 2016).

3.2 | PAD4 is associated with GFAP and is upregulated post-laser injury

Previously, we showed that PAD4 is upregulated during gliosis and colocalized with GFAP filaments in Müller glia in the alkali injury model (Wizeman & Mohan, 2017). Therefore, we determined whether PAD4 is similarly restricted to endfeet or distributed through Müller cell processes and associated with growing polymeric GFAP filaments (Figure 2). In uninjured control retinas, there was weak and diffuse PAD4 staining between the inner nuclear layer (INL) and outer nuclear layer (ONL) (Figure 2a). However, 7 days after injury, a striking pattern of PAD4 expression was evident on Müller glial filaments: PAD4 expression was concurrent and colocalized with GFAP expression. The colocalization of PAD4 on GFAP filaments confirms our prior studies using confocal microscopy (Palko et al., 2022; Wizeman & Mohan, 2017). The staining of GFAP and PAD4 was quantified (see Methods and File S2), and both showed a significant increase in the lesion site compared to uninjured retinas (Figure 2b). Interestingly, PAD4 staining was most prominent in Müller endfeet, and was found tracking the GFAP IFs into the INL with staining also seen in Müller cell soma. As with citrulline/F95 staining, PAD4 staining was also observed on fewer GFAP filaments and prominently at the lesion site. These GFAP-PAD4 positive filaments extend from the endfeet through the INL and vary in length. Comparisons of F95 staining (Figure 1b) and PAD4 staining (Figure 2b) with that of GFAP in the 7-day injured retinas revealed an interesting finding. Both F95 and PAD4 showed similar abundances but significantly

lower abundance than GFAP (GFAP mean rank = 45.50; F95 mean rank = 23.0; PAD4 mean rank = 22.59 with F95 vs. GFAP, $p < .0001$; PAD4 vs. GFAP, $p = .0001$; Kruskal-Wallis nonparametric with Dunn's multiple comparisons test). Collectively, these results reveal that increased PAD4 production correlates with F95 staining in reactive Müller glia and likely drives hypercitrullination in the laser injury model.

3.3 | Soluble GFAP increases in laser-induced retinal gliosis

GFAP hypercitrullination is known to alter filament dynamics and cause GFAP depolymerization in vitro (Inagaki et al., 1989). However, whether citrullinated GFAP that was produced after laser injury remains as a cytoskeletal protein in vivo is unclear. To determine the distribution of soluble and cytoskeletal forms of GFAP after injury (see Methods), we performed western blot analysis of these two fractions from retinas of control and 7- and 16-day post-laser injured mice. The 16-day time point reflects when changes in reactive Müller glia occur in response to alterations in retinal thickness that correspond to the reduction in subretinal edema (Giani et al., 2011). Notably, levels of soluble GFAP were significantly upregulated at 7-day post-injury and trended to remain upregulated at 16-day post-injury compared to control uninjured retinas (Figure 3a,c,e). Interestingly, there were no significant changes in the amount of cytoskeletal GFAP after injury at either time point (Figure 3b,d,f). These results suggest that upon laser injury, the increased cytoskeletal GFAP (visualized by immunostaining) in reactive Müller glia may be unstable, and hence, are extracted into the soluble buffer, thus producing increased amounts of soluble forms of the protein.

3.4 | Soluble citrullinated protein increases in laser-induced retinal gliosis

We next asked whether citrullinated species associated with reactive gliosis were also differentially distributed in soluble and cytoskeletal fractions by laser injury. Using western blot analysis, we determined that several protein species of different sizes were detected in the soluble fraction. In previous studies, we characterized citrullinated isoforms of GFAP using two-dimensional gel analysis (Wizeman et al., 2016). We utilized the same antibody to detect citrullinated species in the laser injury model. A soluble citrullinated protein species at 50 kDa, as shown previously by co-immunoprecipitation studies (Wizeman et al., 2016) is likely citrullinated GFAP (Figure 4a, arrowhead). The intensity of this 50 kDa band increased significantly at 7 days post-injury from control levels and remained significant at 16 days post-injury (Figure 4c). Soluble citrullinated protein species at 75 kDa (Figure 4a, arrow) showed a similar trend showing an increase at 7 days that became significant at 16 days post-injury (Figure 4d). As the size of PAD4 is represented by 75 kDa species, this band is potentially auto-citrullinated PAD4 (Mondal et al., 2021) that is produced post-injury. Lastly, the high molecular weight (HMW) citrullinated proteins (sized >100 kDa, Figure 4a,f, bracket) increased significantly at 7 and 16 days post-injury (Figure 4e,i).

3.5 | Cytoskeletal high molecular weight (HMW) citrullinated proteins increase in laser-induced retinal gliosis

Although soluble citrullinated proteins were increased in focal lesions, we were interested in knowing if any citrullinated species remained stably associated with the cytoskeletal insoluble fraction. We found that HMW citrullinated species in the insoluble cytoskeletal

fraction were significantly increased at 16 days post-injury, as determined by western blot analysis (Figure 4f,i). This could indicate that a pathological state has developed over 16 days, as a similar accumulation of HMW citrullinated proteins was also previously reported in the severe alkali injury model that results in retinal degeneration (Wizeman et al., 2016). Interestingly, HMW citrullinated protein species after laser injury also trended higher in the cytoskeletal fraction at the earlier time point of 7 days but revealed greater complexity (more bands) and became significant at 16 days post-injury (Figure 4f,i), a time point when the 75 kDa citrullinated band showed a dramatic reduction (Figure 4h). The citrullinated 50 kDa GFAP band was barely detected in cytoskeletal extracts from the injured retinas revealing that this protein was readily soluble. These findings further establish that changes in the repertoire of citrullinated targets and their differential distribution between soluble and cytoskeletal fractions occurred at the 16-day post-injury time point.

3.6 | Cytoskeletal PAD4 increases in laser-induced retinal gliosis

Because citrullinated proteins were increased after laser injury, we anticipated that levels of PAD4, the relevant PAD isozyme (Wizeman & Mohan, 2017), would also have increased. We confirmed this by western blot analysis. Soluble PAD4 protein levels showed a trend of increased expression at 7- and 16-day post-injury compared to controls (Figure 5a,c), with significantly increased expression being seen instead in the insoluble cytoskeletal fraction at 16 days post-laser injury (Figure 5b,d). These findings indicate that PAD4 had indeed increased expression contributing to the increased levels of citrullinated proteins. However, increased PAD4 levels preferentially distributed in the cytoskeletal fraction at 16 days post-injury suggested that cytoskeletal-associated PAD4 may represent the fraction of PAD4 that remains non-citrullinated. These data also correlate with PAD4 colocalizing on GFAP filaments as shown here (Figure 2) and previously by immunostaining analysis (Wizeman & Mohan, 2017).

3.7 | Pharmacogenetic ablation of PAD4 reduces hypercitrullination and subretinal fibrosis

Since PAD4 plays a central role in retinal gliosis by governing the stress-induced citrullination of GFAP (Palko et al., 2022; Wizeman & Mohan, 2017), we selectively ablated Padi4 gene expression in glial cells by crossing GFAP-CreERT2 with Padi4flox/flox mice and administering tamoxifen to induce PAD4 deficiency (PAD4cKO mice). Our earlier study revealed that citrullinated GFAP levels, abundantly expressed after injury were reduced in PAD4 deficiency (Palko et al., 2022). Moreover, western blot analysis also confirmed significant reductions of several hypercitrullinated species that correlated with reductions in PAD4 protein levels in injured PAD4cKO retinas (Palko et al., 2022). These findings, therefore, prompted us to examine the consequences of PAD4cKO on laser-injury chronic gliosis and hypercitrullination with relevance to subretinal fibrosis at the 30-day time point post-injury (Ishikawa et al., 2016). Immunostaining analysis of mouse retinas 30 days post-laser injury revealed that filamentous GFAP was abundant in Müller glial processes and visualized extending to the outer nuclear layer of lesion sites of injured control retinas (Figure 6). These long $GFAP^+$ filaments showed a high level of overlap with citrullination (F95) staining (mean GFAP = 121.9 ± 45.19; mean F95 = 122.2 ± 44.96; Mann–Whitney test, $U = 0$, $n_1 = 17$, $n_2 = 17$, $p = .9458$). This finding suggested that by

30 days post-injury GFAP stained filaments in lesioned areas were completely marked by citrullination (hypercitrullinated). In comparison, GFAP staining in the injured PAD4cKO retinas was more restricted, with staining for GFAP in Müller cell processes reaching only the inner nuclear layer and being relatively sparse. Notably, citrullinated species were largely undetected in PAD4cKO retinas by immunostaining (Figure 6). The staining of F95 was quantified and showed very significant decrease in citrullinated species in the PAD4cKO mice compared to the control (Figure 6e). This reduction of citrullination staining correlated with that previously observed by western blot analysis (Palko et al., 2022). Thus, loss of filamentous citrullinated species in PAD4cKO retinas indicates that PAD4 enzymatic activity may be integral to the maintenance of hypercitrullination at this chronic stage of injury. GFAP staining quantification also showed significant reduction in PAD4cKO mice compared to controls, although not to the same extent as that of F95 (Figure 6e). Therefore, next we wanted to determine whether conditional glial-specific targeting of PAD4 reversed structural changes in the injured retina that would be reflected by alterations to GFAP filaments within Müller glia (Bringmann et al., 2009). To examine this, we quantified lesion size using live fundus imaging of laser-injured mice 30 days post-injury. We found that lesion sizes differed significantly between control (mean = 3.003 ± 0.4988) and PAD4cKO (mean = 2.058 ± 0.5147) injured mice (Mann–Whitney U test, $p < .0001$, Figure 7b), suggesting that there may be improvement in tissue repair in PAD4 deficiency. These data prompted us to examine whether lesion-associated subretinal fibrosis (Ishikawa et al., 2016), as reflected by the amount of fibronectin deposition (Linder et al., 2021), was also affected by PAD4 conditional knockout. PAD4cKO and control retinas 30 days post-injury were immunostained for fibronectin, and we measured areas of subretinal staining at lesion sites (Figure 8, see File S2). We found that the PAD4cKO injured retinas had a very significant reduction in fibronectin staining (mean = 0.3764 ± 0.1005) compared to the high amount of fibronectin in the control injured retinas (mean = 2.219 ± 0.4313) (Welch's parametric t test, $p < .0001$; Figure 8e,f). Taken together, these findings reveal that PAD4 overexpression in reactive Müller glia plays an important role in the development of subretinal fibrosis. This indicates that chronically reactive Müller glia may be responsible for perpetuating the fibrotic outcome via engaging the PAD4-citrullination axis.

4 | DISCUSSION

Fibrotic scarring is associated with chronic retinal gliosis and remains an inevitable outcome in ~45% of patients with advanced wet-AMD (Daniel et al., 2014). We recently reported that retinal gliosis elicited in the mouse laser injury model of accelerated CNV is associated with PAD4-driven hypercitrullination. We illuminated that injury-induced PAD4 upregulation governed the production of citrullinated GFAP, and this citrullination originates from Müller endfeet (Palko et al., 2022). Here we show, for the first time, that in conditional PAD4-deficient retinas, laser-induced Müller glial hypercitrullination was reduced dramatically on a global level, resulting in altered GFAP production and attenuated subretinal fibrosis.

One of the earliest hallmarks of retinal gliosis is the de novo production of GFAP in Müller glia (Lewis & Fisher, 2003), entailing Gfap mRNA synthesis and its transport to the endfeet for translation (Sarthy et al., 1989). Soluble GFAP produced in the endfeet is polymerized rapidly as the filamentous forms of GFAP are observed very early after injury (Wizeman

et al., 2016). We have shown these polymeric GFAP filaments are also citrullinated at the endfeet and previously posited that the cellular components to drive translation (Sarthy et al., 1989) and citrullination may be present in the endfeet (Palko et al., 2022). As immunostaining showed the colocalization of PAD4 at the endfeet, we believe that the PAD4-citrullination axis is intimately linked to Müller cell gliosis. This finding was novel because PAD4 has never been colocalized with any of its intermediate filament substrates in such a compartmentalized manner. This also exemplifies that this unique mechanism may be a construct of biology to serve the polarized structure of the neurosensory retina. Thus, we speculate that initiating stress-induced citrullination at Müller cell endfeet, an anatomical site located distally from photoreceptors, could be a protective strategy to promote repair after a minor injury. This way, acute gliosis could occur concurrently without disruption of phototransduction in the photoreceptor outer segments. However, in events of severe traumatic injury or genetic diseases producing a permanent protein deficit/abnormality, the ensuing chronic retinal gliosis would provide a conduit for Müller cell-mediated transport of PAD4 through cell processes via the cytoskeleton. Under such a pathological scenario, the repertoire of citrullinated species would increase both in abundance and complexity. Thus, the chronically activated Müller would continue to produce these citrullinated proteins at the endfeet that would impact outer retinal layers to cause degeneration. In support of this idea, JR5558 mice that spontaneously develop retinal degeneration from lesions that arise in defective photoreceptor outer segments (Chang et al., 2018) were found to have robust gliosis with highly citrullinated filaments that extended all the way to the apical end of Müller glia by 1 month of age (Palko et al., 2022). Also, in laser-injured mouse retinas, citrullinated filaments extended to the apical end of Müller glia (Palko et al., 2022), which correlated with temporal changes in the abundance and pattern of citrullinated proteins produced over the 16-day-injury period. Thus, the spread of citrullination from the endfeet to the outer retina and its temporal retention appears to manifest when acute gliosis fails to resolve. As such, the endfeet should be recognized as a critical subcellular domain compartmentalized to drive retinal citrullination in both the acute and chronic stages of pathology. This idea is consistent with our recent findings that showed citrullinated GFAP in the endfeet of human wet-AMD maculae with chronic gliosis at this advanced stage of fibrosis (Palko et al., 2022). Accordingly, we have named the endfeet of reactive Müller glia the “citrullination bunker” (Palko et al., 2022).

To better understand the structural regulation of GFAP via its citrullination, we analyzed retinal extracts at 7- and 16-day post-injury using western blots. Our findings reveal that the temporal increase in GFAP and citrullinated species occurs both in the soluble and cytoskeletal fractions, suggesting that immunostained filamentous citrullinated GFAP contains a certain number of unstable subunits that were readily solubilized. While these data are illuminating, limitations of our study are that some data (western blots) that have lent support to our results were derived from small sample sizes. Also, the nature of the interactions of PAD4 with GFAP is ambiguous. However, these observations still provide a basis for hypothesis testing should such a PAD4-GFAP binding interaction be found to be true. Then, the dramatic loss in the 75 kDa citrullinated PAD4 species in the cytoskeletal fraction at the 16-day time point suggests auto-citrullinated PAD4 (Wizeman & Mohan, 2017) is being released from polymeric GFAP at later stages in injury. In apposition

to this idea, increased abundance of PAD4 in the cytoskeletal fraction indicates that an inverse relationship may exist; PAD4 decreases its binding to polymeric GFAP when PAD4 becomes increasingly auto-citrullinated. Thus, PAD4 auto-citrullination may not only cause autoinhibition of PAD4 enzymatic activity (Mondal et al., 2021), but auto-citrullination of PAD4 may also be a breaking mechanism to limit the amount of activated PAD4 being chaperoned in the direction of the outer nuclear layer on the IF cytoskeleton. Future studies will be needed to define how potential interactions of PAD4 with GFAP are altered as a reflection of citrullination during the polymerization and dynamic remodeling of GFAP filamentous structures. Alternatively, one might anticipate that dynamic changes also in cell size and shape of reactive Müller glia would correspondingly require GFAP polymers to adapt to alterations in cell stiffness and retinal thickness (Middeldorp & Hol, 2011) that continue to occur even at later time points post-laser injury (Giani et al., 2011). Future studies could help illuminate whether hypercitrullination of GFAP drives these cellular alterations or are the result of such structural alterations to the retina. Finally, other substrates of PAD4 that potentially govern Müller glial cell biological processes need to be identified and characterized, which is an important study that remains to be done.

Conditional abrogation of PAD4 in Müller glia reduces GFAP polymeric expression, as much shorter and sparser GFAP filaments were detected 30-day post-injury in PAD4cKO mice compared to injured controls. The dramatic reduction in retinal lesion size in PAD4cKO mice hints that hypercitrullination may be driving structural changes in the injured retinas. One thought is that the lesioned areas of the retina may undergo tissue remodeling more effectively because of attenuated citrullination. Global reduction of citrullinated protein species was also significant at 16 days post-injury in laser injured PAD4cKO retinas compared to injured controls (Palko et al., 2022), suggesting that downregulation of hypercitrullination and maintenance of low level of gliosis could be beneficial for repair over pathological engagement of fibrosis. In keeping with this, the consequence of attenuation of the PAD4-citrullination axis results in significantly diminished subretinal fibrosis (lower fibronectin levels), which corroborates a role for PAD4 in retinal fibrosis. As such, PAD4 deficiency or its inhibition in several other animal models of fibrotic conditions have resulted in protection (Kawalkowska et al., 2016; Knight et al., 2015; Lange et al., 2014; Suzuki et al., 2020; Vassiliadis et al., 2013), identifying this PAD enzyme as a major player in fibrosis. Moreover, the consequence of PAD4 overexpression could also eventually lead to development of immune deviation through generation of autoantibodies to PAD4 (Acharya et al., 2012), as well as to GFAP (Darrah & Andrade, 2018), or to other PAD4 substrates, which ultimately could be factors that exacerbate the disease process. Nevertheless, while our study focuses solely on reactive Müller glia, astrocytes may also contribute to gliosis in this injury model in other ways, but it is unlikely that astrocytes located at the GCL influence subretinal fibrosis.

Together, our findings on the PAD4-citrullination axis in Müller cell gliosis suggest a potential role for PAD4 in AMD through effects on the fibrotic process (Palko et al., 2022). Whether this mechanism also interferes with CNV now remains to be tested. As PAD4 is also a therapeutic target in other chronic diseases (Jones et al., 2009), future studies should investigate the impact of pharmacological inhibition of PAD4 on disease progression in the retina.

Supplementary Material

Refer to Web version on PubMed Central for supplementary material.

ACKNOWLEDGMENTS

The authors wish to thank Katie Lowther and Deborah Kaback from the Center for Mouse Genome Modification for their assistance with transgenic mouse breeding experiments and colony management.

FUNDING INFORMATION

This research was funded by NIH grant R21EY028699 and the John A. and Florence Mattern Solomon endowed chair to R.M. The opinions and assertions contained herein are the private opinions of the authors and are not to be construed as reflecting the views of University of Connecticut Health Center, the National Institutes of Health, or the UConn Foundation.

Funding information

NIH R21EY028699; John A. and Florence Mattern Solomon endowed chair

DATA AVAILABILITY STATEMENT

The Supplemental files contain additional information to support the findings. For reasonable requests of any additional information please contact the corresponding author.

REFERENCES

Acharya NK, Nagele EP, Han M, Coretti NJ, DeMarshall C, Kosciuk MC, Boulos PA, & Nagele RG (2012). Neuronal PAD4 expression and protein citrullination: Possible role in production of autoantibodies associated with neurodegenerative disease. Journal of Autoimmunity, 38(4), 369–380. 10.1016/j.jaut.2012.03.004 [PubMed: 22560840]

Ambati J, Ambati BK, Yoo SH, Ianchulev S, & Adamis AP (2003). Age-related macular degeneration: Etiology, pathogenesis, and therapeutic strategies. Survey of Ophthalmology, 48(3), 257–293. 10.1016/s0039-6257(03)00030-4 [PubMed: 12745003]

Bargagna-Mohan P, Paranthan RR, Hamza A, Dimova N, Trucchi B, Srinivasan C, Elliott GI, Zhan C-G, Lau DL, Zhu H, Kasahara K, Inagaki M, Cambi F, & Mohan R (2010). Withaferin a targets intermediate filaments glial fibrillary acidic protein and vimentin in a model of retinal gliosis. Journal of Biological Chemistry, 285(10), 7657–7669. 10.1074/jbc.M109.093765 [PubMed: 20048155]

Bonilha VL, Shadrach KG, Rayborn ME, Li Y, Pauer GJ, Hagstrom SA, Bhattacharya SK, & Hollyfield JG (2013). Retinal deimination and PAD2 levels in retinas from donors with age-related macular degeneration (AMD). Experimental Eye Research, 111, 71–78. 10.1016/j.exer.2013.03.017 [PubMed: 23562679]

Bringmann A, Iandiev I, Pannicke T, Wurm A, Hollborn M, Wiedemann P, Osborne NN, & Reichenbach A (2009). Cellular signaling and factors involved in muller cell gliosis: Neuroprotective and detrimental effects. Progress in Retinal and Eye Research, 28(6), 423–451. 10.1016/j.preteyeres.2009.07.001 [PubMed: 19660572]

Bringmann A, & Wiedemann P (2012). Muller glial cells in retinal disease. Ophthalmologica, 227(1), 1–19. 10.1159/000328979

Briot J, Simon M, & Mechin MC (2020). Deimination, intermediate filaments and associated proteins. International Journal of Molecular Sciences, 21(22), 8746. 10.3390/ijms21228746 [PubMed: 33228136]

Chang B, FitzMaurice B, Wang J, Low BE, Wiles MV, & Nishina PM (2018). Spontaneous posterior segment vascular disease phenotype of a mouse model, rnv3, is dependent on the Crb1rd8 allele. Investigative Ophthalmology & Visual Science, 59(12), 5127–5139. 10.1167/iovs.18-25046 [PubMed: 30372741]

Daniel E, Toth CA, Grunwald JE, Jaffe GJ, Martin DF, Fine SL, Huang J, Ying G, Hagstrom SA, Winter K, Maguire MG, & Comparison of Age-related Macular Degeneration Treatments Trials Research Group. (2014). Risk of scar in the comparison of age-related macular degeneration treatments trials. Ophthalmology, 121(3), 656–666. 10.1016/j.ophtha.2013.10.019 [PubMed: 24314839]

Darrah E, & Andrade F (2018). Rheumatoid arthritis and citrullination. Current Opinion in Rheumatology, 30(1), 72–78. 10.1097/BOR.0000000000000452 [PubMed: 28937414]

Edwards MM, McLeod DS, Bhutto IA, Grebe R, Duffy M, & Lutty GA (2017). Subretinal glial membranes in eyes with geographic atrophy. Investigative Ophthalmology & Visual Science, 58(3), 1352–1367. 10.1167/iovs.16-21229 [PubMed: 28249091]

Eriksson JE, He T, Trejo-Skalli AV, Harmala-Brasken AS, Hellman J, Chou YH, & Goldman RD (2004). Specific in vivo phosphorylation sites determine the assembly dynamics of vimentin intermediate filaments. Journal of Cell Science, 117(Pt 6), 919–932. 10.1242/jcs.00906 [PubMed: 14762106]

Fabian-Jessing BK, Jakobsen TS, Jensen EG, Alsing S, Hansen S, Aagaard L, Askou AL, Bek T, & Corydon TJ (2022). Animal models of choroidal neovascularization: A systematic review. Investigative Ophthalmology & Visual Science, 63(9), 11. 10.1167/iovs.63.9.11

Giani A, Thanos A, Roh MI, Connolly E, Trichonas G, Kim I, Gragoudas E, Vavvas D, & Miller JW (2011). In vivo evaluation of laser-induced choroidal neovascularization using spectral-domain optical coherence tomography. Investigative Ophthalmology & Visual Science, 52(6), 3880–3887. 10.1167/iovs.10-6266 [PubMed: 21296820]

Hippert C, Graca AB, Basche M, Kalargyrou AA, Georgiadis A, Ribeiro J, Matsuyama A, Aghaizu N, Bainbridge JW, Smith AJ, Ali RR, & Pearson RA (2021). RNAi-mediated suppression of vimentin or glial fibrillary acidic protein prevents the establishment of muller glial cell hypertrophy in progressive retinal degeneration. Glia, 69(9), 2272–2290. 10.1002/glia.24034 [PubMed: 34029407]

Hol EM, & Capetanaki Y (2017). Type III intermediate filaments desmin, glial fibrillary acidic protein (GFAP), vimentin, and peripherin. Cold Spring Harbor Perspectives in Biology, 9(12), a021642. 10.1101/cshperspect.a021642 [PubMed: 29196434]

Hollingsworth TJ, Radic MZ, Beranova-Giorgianni S, Giorgianni F, Wang Y, & Iannaccone A (2018). Murine retinal citrullination declines with age and is mainly dependent on peptidyl arginine deiminase 4 (PAD4). Investigative Ophthalmology & Visual Science, 59(10), 3808–3815. 10.1167/iovs.18-24118 [PubMed: 30073354]

Inagaki M, Takahara H, Nishi Y, Sugawara K, & Sato C (1989). Ca^{2+}-dependent deimination-induced disassembly of intermediate filaments involves specific modification of the amino-terminal head domain. Journal of Biological Chemistry, 264(30), 18119–18127. [PubMed: 2808368]

Ishikawa K, Kannan R, & Hinton DR (2016). Molecular mechanisms of subretinal fibrosis in age-related macular degeneration. Experimental Eye Research, 142, 19–25. 10.1016/j.exer.2015.03.009 [PubMed: 25773985]

Jones JE, Causey CP, Knuckley B, Slack-Noyes JL, & Thompson PR (2009). Protein arginine deiminase 4 (PAD4): Current understanding and future therapeutic potential. Current Opinion in Drug Discovery & Development, 12(5), 616–627. [PubMed: 19736621]

Kawalkowska J, Quirke AM, Ghari F, Davis S, Subramanian V, Thompson PR, Williams RO, Fischer R, La Thangue NB, & Venables PJ (2016). Abrogation of collagen-induced arthritis by a peptidyl arginine deiminase inhibitor is associated with modulation of T cell-mediated immune responses. Scientific Reports, 6, 26430. 10.1038/srep26430 [PubMed: 27210478]

Knight JS, Subramanian V, O'Dell AA, Yalavarthi S, Zhao W, Smith CK, Hodgin JB, Thompson PR, & Kaplan MJ (2015). Peptidylarginine deiminase inhibition disrupts NET formation and protects against kidney, skin and vascular disease in lupus-prone MRL/lpr mice. Annals of the Rheumatic Diseases, 74(12), 2199–2206. 10.1136/annrheumdis-2014-205365 [PubMed: 25104775]

Lange S, Rocha-Ferreira E, Thei L, Mawjee P, Bennett K, Thompson PR, Subramanian V, Nicholas AP, Peebles D, Hristova M, & Raivich G (2014). Peptidylarginine deiminases: Novel drug targets for prevention of neuronal damage following hypoxic ischemic insult (HI) in neonates. Journal of Neurochemistry, 130(4), 555–562. 10.1111/jnc.12744 [PubMed: 24762056]

Lewis GP, & Fisher SK (2003). Up-regulation of glial fibrillary acidic protein in response to retinal injury: Its potential role in glial remodeling and a comparison to vimentin expression. International Review of Cytology, 230, 263–290. 10.1016/s0074-7696(03)30005-1 [PubMed: 14692684]

Lewis HD, Liddle J, Coote JE, Atkinson SJ, Barker MD, Bax BD, Bicker KL, Bingham RP, Campbell M, Chen YH, Chung C-W, Craggs PD, Davis RP, Eberhard D, Joberty G, Lind KE, Locke K, Maller C, Martinod K, … Wilson DM (2015). Inhibition of PAD4 activity is sufficient to disrupt mouse and human NET formation. Nature Chemical Biology, 11(3), 189–191. 10.1038/nchembio.1735 [PubMed: 25622091]

Linder M, Foxton R, Uhles S, Revelant F, Lazendic M, Canonica J, Garrido MG, & Westenskow P (2021). Simultaneous Ang-2/VEGF-A inhibition prevents subretinal fibrosis progression in preclinical mouse models of choroidal neovascularization (CNV). Investigative Ophthalmology & Visual Science, 62(8), 349.

Liu Y, Kanda A, Wu D, Ishizuka ET, Kase S, Noda K, Ichihara A, & Ishida S (2019). Suppression of choroidal neovascularization and fibrosis by a novel RNAi therapeutic agent against (pro)renin receptor. Molecular Therapy–Nucleic Acids, 17, 113–125. 10.1016/j.omtn.2019.05.012 [PubMed: 31254924]

Middeldorp J, & Hol EM (2011). GFAP in health and disease. Progress in Neurobiology, 93(3), 421–443. 10.1016/j.pneurobio.2011.01.005 [PubMed: 21219963]

Mondal S, Wang S, Zheng Y, Sen S, Chatterjee A, & Thompson PR (2021). Site-specific incorporation of citrulline into proteins in mammalian cells. Nature Communications, 12(1), 45. 10.1038/s41467-020-20279-w

Nicholas AP, Sambandam T, Echols JD, & Tourtellotte WW (2004). Increased citrullinated glial fibrillary acidic protein in secondary progressive multiple sclerosis. Journal of Comparative Neurology, 473(1), 128–136. 10.1002/cne.20102 [PubMed: 15067723]

Palko SI, Saba NJ, Mullane E, Nicholas BD, Nagasaka Y, Ambati J, Gelfand BD, Ishigami A, Bargagna-Mohan P, & Mohan R (2022). Compartmentalized citrullination in muller glial endfeet during retinal degeneration. Proceedings of the National Academy of Sciences of the United States of America, 119(9), e2121875119. 10.1073/pnas.2121875119 [PubMed: 35197297]

Rivero-Gutierrez B, Anzola A, Martinez-Augustin O, & de Medina FS (2014). Stain-free detection as loading control alternative to ponceau and housekeeping protein immunodetection in Western blotting. Analytical Biochemistry, 467, 1–3. 10.1016/j.ab.2014.08.027 [PubMed: 25193447]

Sarthy PV, Fu M, & Huang J (1989). Subcellular localization of an intermediate filament protein and its mRNA in glial cells. Molecular and Cellular Biology, 9(10), 4556–4559. 10.1128/mcb.9.10.4556-4559.1989 [PubMed: 2586519]

Suzuki M, Ikari J, Anazawa R, Tanaka N, Katsumata Y, Shimada A, Suzuki E, & Tatsumi K (2020). PAD4 deficiency improves bleomycin-induced neutrophil extracellular traps and fibrosis in mouse lung. American Journal of Respiratory Cell and Molecular Biology, 63(6), 806–818. 10.1165/rcmb.2019-0433OC [PubMed: 32915635]

Telegina DV, Kozhevnikova OS, & Kolosova NG (2018). Changes in retinal glial cells with age and during development of age-related macular degeneration. Biochemistry, 83(9), 1009–1017. 10.1134/S000629791809002X [PubMed: 30472939]

van Bodegraven EJ, & Etienne-Manneville S (2021). Intermediate filaments from tissue integrity to single molecule mechanics. Cells, 10(8), 1905. 10.3390/cells10081905 [PubMed: 34440673]

Vassiliadis E, Veidal SS, Kristiansen MN, Hansen C, Jorgensen M, Leeming DJ, & Karsdal M (2013). Peptidyl arginine deiminase inhibitor effect on hepatic fibrogenesis in a CCl4 pre-clinical model of liver fibrosis. American Journal of Translational Research, 5(4), 465–469. [PubMed: 23724169]

Verardo MR, Lewis GP, Takeda M, Linberg KA, Byun J, Luna G, Wilhelmsson U, Pekny M, Chen D-F, & Fisher SK (2008). Abnormal reactivity of muller cells after retinal detachment in mice deficient in GFAP and vimentin. Investigative Ophthalmology & Visual Science, 49(8), 3659–3665. 10.1167/iovs.07-1474 [PubMed: 18469190]

Willis VC, Banda NK, Cordova KN, Chandra PE, Robinson WH, Cooper DC, Lugo D, Mehta G, Taylor S, Tak PP, Prinjha RK, Lewis HD, & Holers VM (2017). Protein arginine deiminase 4 inhibition is sufficient for the amelioration of collagen-induced arthritis. Clinical and Experimental Immunology, 188(2), 263–274. 10.1111/cei.12932 [PubMed: 28128853]

Witalison EE, Thompson PR, & Hofseth LJ (2015). Protein arginine deiminases and associated citrullination: Physiological functions and diseases associated with dysregulation. Current Drug Targets, 16(7), 700–710. 10.2174/1389450116666150202160954 [PubMed: 25642720]

Wizeman JW, & Mohan R (2017). Expression of peptidylarginine deiminase 4 in an alkali injury model of retinal gliosis. Biochemical and Biophysical Research Communications, 487(1), 134–139. 10.1016/j.bbrc.2017.04.031 [PubMed: 28400047]

Wizeman JW, Nicholas AP, Ishigami A, & Mohan R (2016). Citrullination of glial intermediate filaments is an early response in retinal injury. Molecular Vision, 22, 1137–1155. [PubMed: 27703308]

Wu KH, Madigan MC, Billson FA, & Penfold PL (2003). Differential expression of GFAP in early v late AMD: A quantitative analysis. British Journal of Ophthalmology, 87(9), 1159–1166. 10.1136/bjo.87.9.1159 [PubMed: 12928288]

Significance

This research study is significant because it contains novel information about a potential mechanism that links retinal Müller glial hypercitrullination to subretinal fibrosis. We show that functional reduction of PAD4 that abrogates hypercitrullination improves retinal injury and diminishes subretinal fibrosis, potentially through its effects on GFAP dynamics. These new data are important for consideration of scarring in retinal diseases like age-related macular degeneration as its also illuminates PAD4 as a potential drug-gable target for fibrotic conditions.

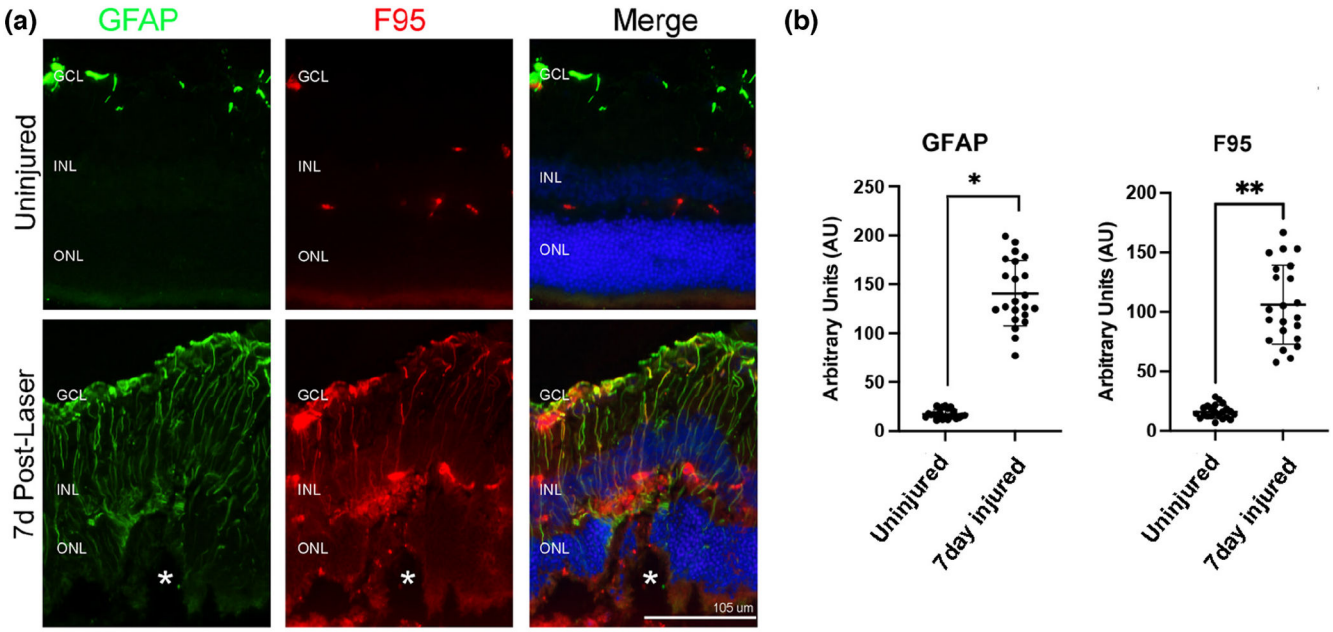

FIGURE 1.

Citrullination colocalizes with GFAP filaments in laser-injured mouse retinas. (a) Representative epifluorescent images of control uninjured and 7-day post-laser injury retinal samples stained for GFAP (green) and peptidyl-citrulline/F95 (red). Nuclei were visualized with DAPI (blue). Citrullinated proteins were present on filaments and colocalized with GFAP. Merge is an overlay of all staining. All images were taken at 20× magnification. GCL, ganglion cell layer; INL, inner nuclear layer; ONL, outer nuclear layer. The asterisks (a) denote the site of the laser lesion. (b) Quantification of GFAP and F95 staining was done using ImageJ software and data analyzed using graph pad Prism software. The Mann–Whitney two-tailed nonparametric test was used for statistical analysis. Median GFAP abundance of uninjured and 7-day injured samples were 16.36 and 129.8, respectively; the two groups differed significantly ($U = 0$, $n_1 = n_2 = 22$, $^*p < .0001$). Median F95 abundance of uninjured and 7-day injured samples were 14.91 and 98.48, respectively; the two groups differed significantly ($U = 0$, $n_1 = n_2 = 22$, $^{**}p < .0001$). $N = 6$ mice/group, average of three sections per mouse. Data are presented as mean ± SD, $p < .05$ is considered significant. Scale bar = 105 μm.

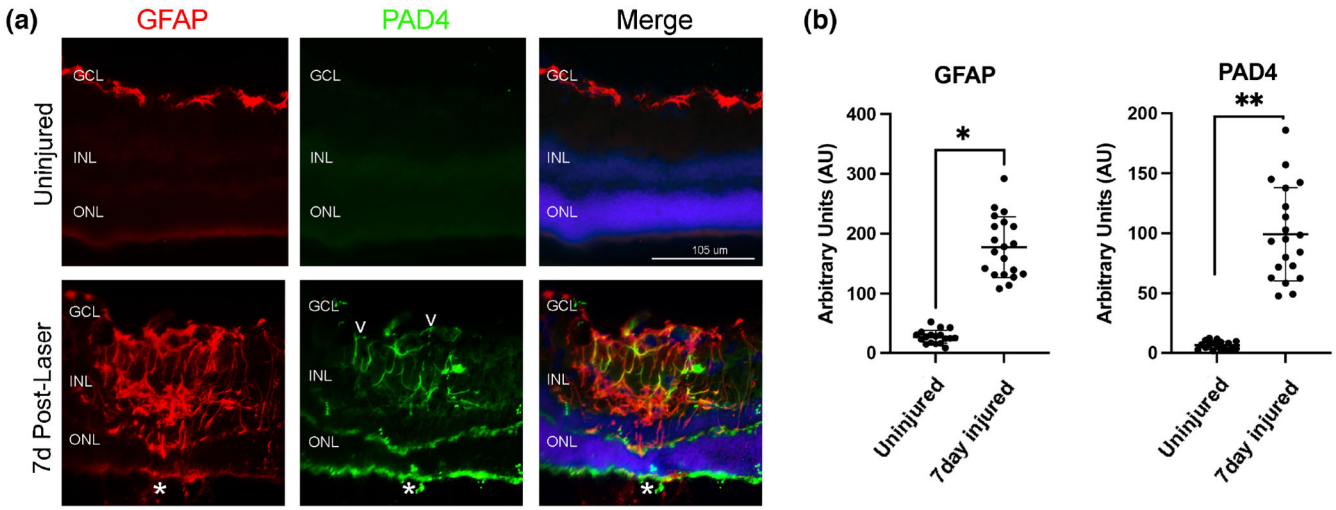

FIGURE 2.

PAD4 is upregulated and localized with GFAP in the injured mouse retina. (a) Representative epifluorescent images of control uninjured and 7-day post-injury retinal samples stained for GFAP (red), PAD4 (green). Nuclei were visualized with DAPI (blue). PAD4 staining was observed colocalized with GFAP filaments originating from the endfeet (white empty arrowheads) and extending to the inner retina of injured tissues. Merge is an overlay of all staining. All images were taken at 20× magnification. GCL, ganglion cell layer; INL, inner nuclear layer; ONL, outer nuclear layer. The asterisks (a) denote the site of the laser lesion. (b) Quantification of GFAP and PAD4 staining was done using ImageJ software and data analyzed using graph PAD Prism software. The Mann–Whitney two-tailed nonparametric test was used for statistical analysis. Median GFAP abundance of uninjured and 7-day injured samples was 26.68 and 174.0, respectively; the two groups differed significantly ($U = 0$, $n_1 = 18$, $n_2 = 20$, $^*p < .0001$). Median PAD4 abundance of uninjured and 7-day injured samples was 6.15 and 94.40, respectively; the two groups differed significantly ($U = 0$, $n_1 = 18$, $n_2 = 20$, $^{**}p < .0001$). $N = 6$ mice/group, average of three sections per mouse. Data are presented as mean ± SD, $p < .05$ is considered significant. Scale bar = 105 μm.

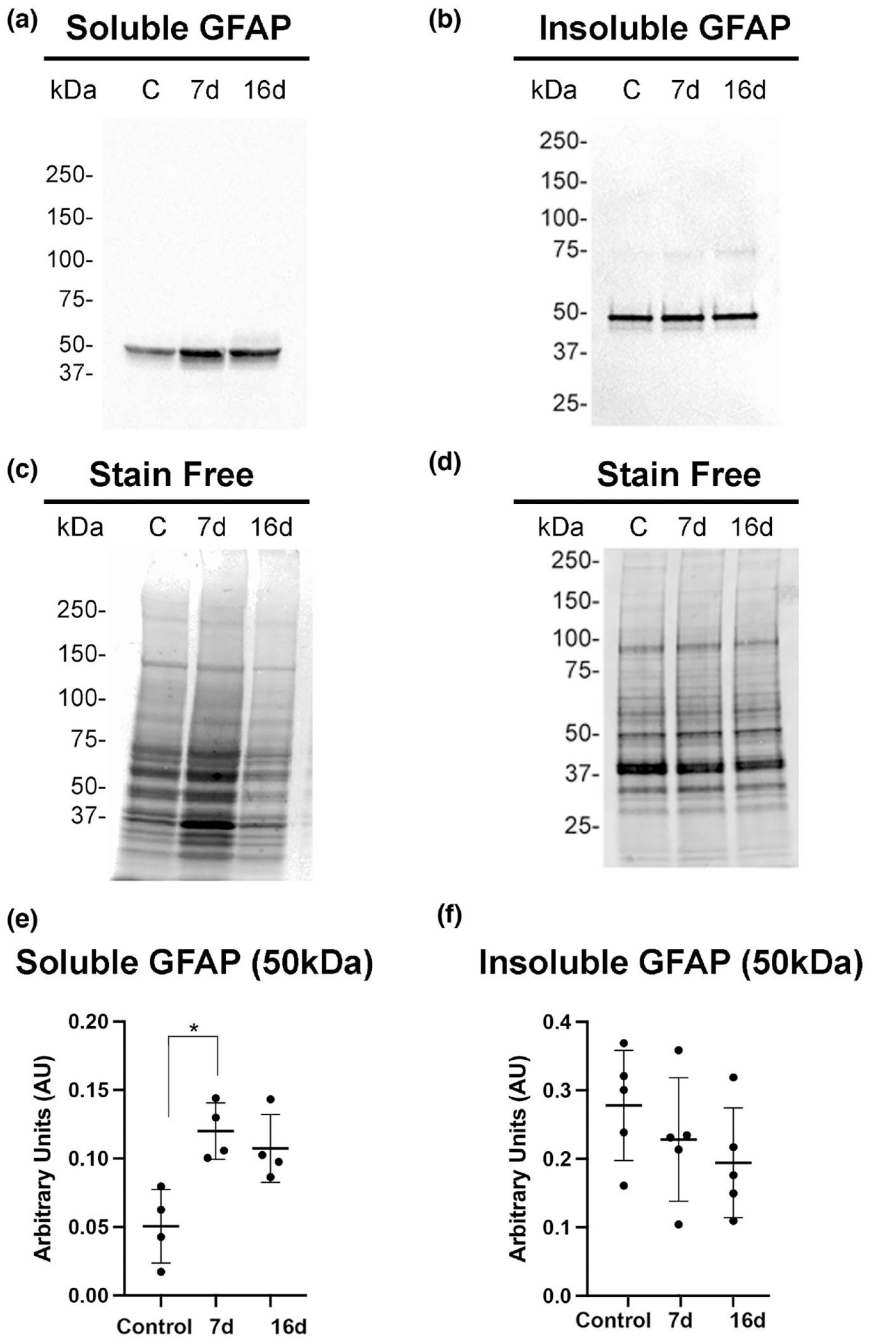

FIGURE 3.

Soluble GFAP increases in mouse retinas after laser injury. Soluble (a) and insoluble (b) cytoskeletal fraction were isolated from control uninjured and injured retinas (7- and 16-day post-injury) and subjected to western blot analysis. Blots were probed with GFAP antibody. (c,d) Stain-free gels were used as protein loading controls. Quantitation of GFAP bands normalized to stain-free gels was done using ImageJ software and data analyzed using GraphPad Prism software. (e) The Kruskal–Wallis test with Dunn's multiple comparisons revealed a statistically significant difference of soluble GFAP abundance between uninjured and 7-day injured samples, $H(2, N = 12) = 8.0$; $*p = .0121$, but the 16-day injured

sample did not show significant differences ($p = .0997$) ($N = 10$ mice/group). (f) The Kruskal–Wallis test with Dunn's multiple comparisons did not reveal statistically significant differences for cytoskeletal GFAP abundance between uninjured and 7-day or 16-day injured samples, $H(2, N = 15) = 2.94$; $p = .256$. Data are presented as mean ± SD, $p < .05$ is considered significant.

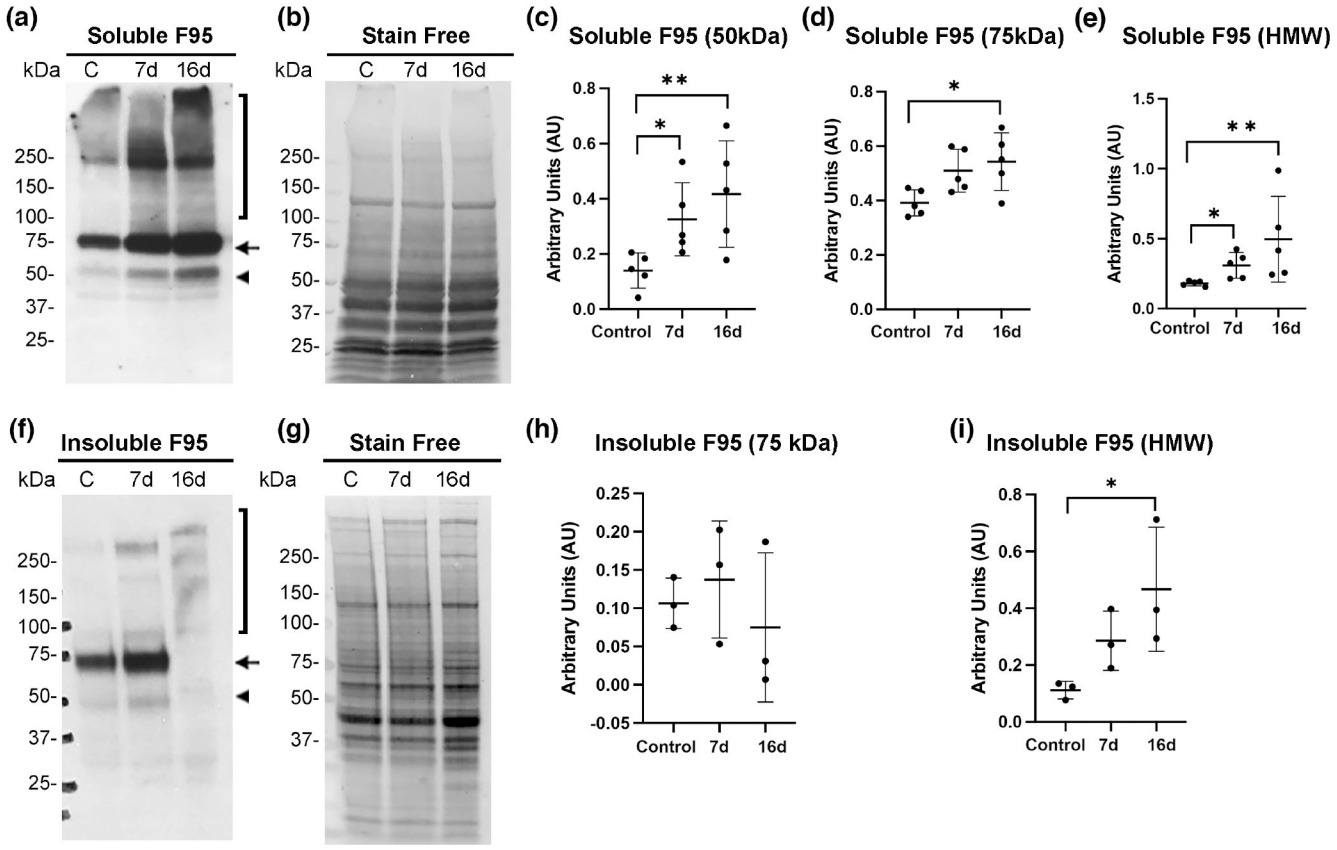

FIGURE 4.

Soluble citrullinated proteins increase in mouse retinas after laser injury. Soluble and insoluble cytoskeletal fractions were isolated from control uninjured and injured retinas (7- and 16-day post-injury) and subjected to western blot analysis. Blots were probed with citrullination/F95 antibody. (a) Multiple soluble bands were visualized at 50 kDa (arrowhead), 75 kDa (arrow), and >100 kDa (HMW, bracket). Quantitation of soluble F95 bands normalized to stain-free gels (b) was done using ImageJ software and data analyzed using GraphPad Prism software. Kruskal–Wallis test with Dunn's multiple comparisons was performed for data from individual bands. Compared to the uninjured sample the soluble 50 kDa band (c) was significantly increased at 7 days post-injury $H(2, N = 15) = 8.06$; $^{*}p = .0473$, and at 16 days post-injury; $^{*}p = .0178$. The abundance of the 75 kDa band (d) increased significantly at 16 days post-injury, $H(2, N = 15) = 6.860$; $^{*}p = .0267$, but not at 7 days post-injury ($p = .0954$). (e) Soluble high molecular weight (HMW) species were also significantly increased at 7 days, $H(2, N = 15) = 9.980$; $^{*}p = .0473$) and at 16 days post-injury ($^{**}p = .0047$). (f) Multiple bands from the cytoskeletal extracts were visualized; 75 kDa (arrow) and several above 100 kDa (HMW, bracket). (g) Stain-free gels were used as protein loading controls for normalization of bands. (h) Compared to the uninjured sample the 75 kDa band from the insoluble fraction at 7- and 16-day post-injury did not show significant differences, $H(2, N = 9) = 1.422$; $p = .5429$ ($N = 6$ mice/group). (i) Quantitation of the HMW bands from the insoluble fraction revealed significant increase at 16-day post-injury, $H(2, N = 9) = 5.956$; $^{*}p = .0341$ but not at 7-day post-injury ($p = .2021$). $N = 6$ mice/group. Data are presented as mean ± SD, $p < .05$ is considered significant.

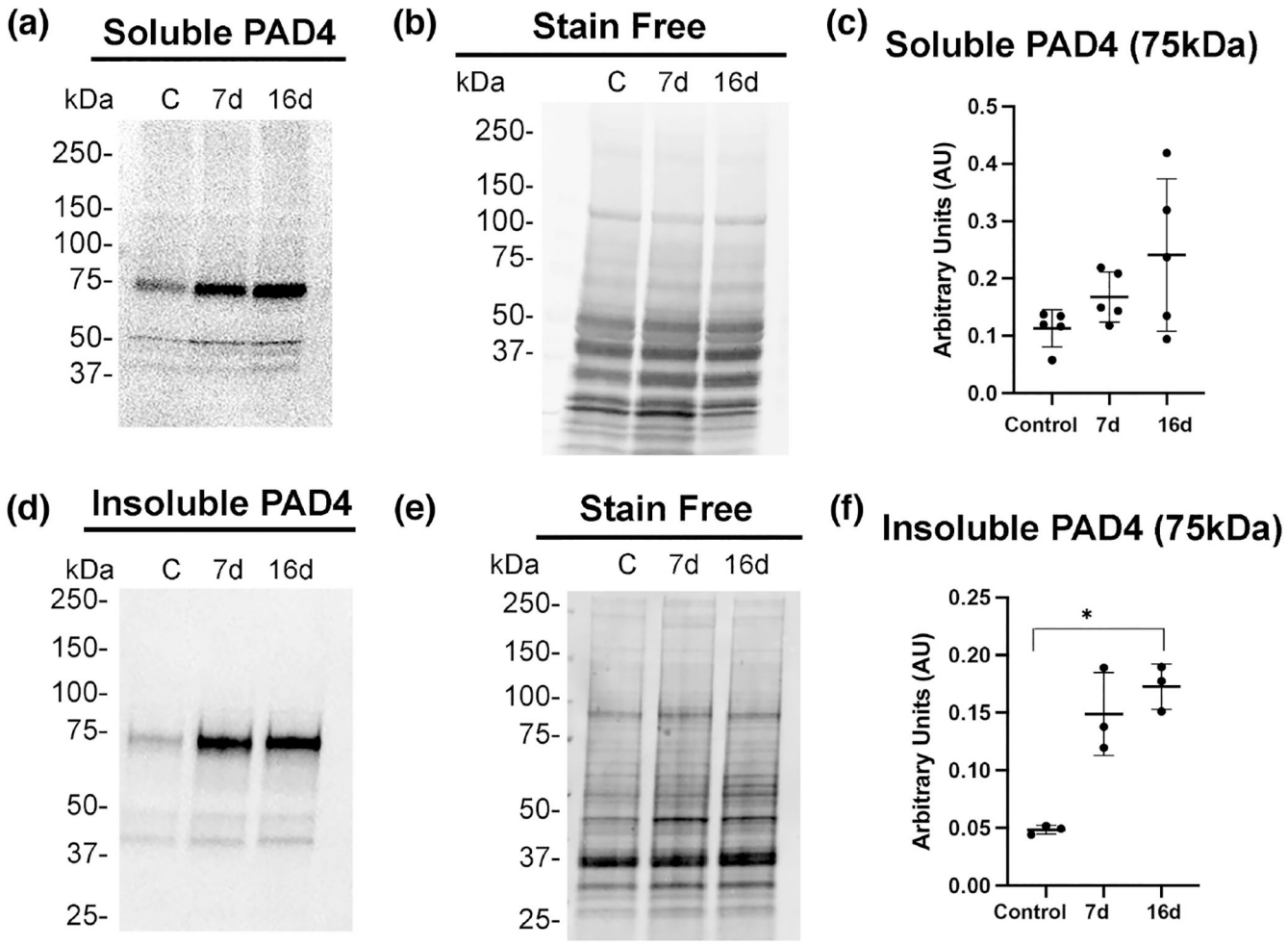

FIGURE 5.

PAD4 increases in the insoluble cytoskeletal fraction in laser injured retinas. Soluble (a) and cytoskeletal (d) fractions were isolated from control uninjured and injured retinas (7- and 16-day post-injury) and analyzed by western blot analysis. Blots were probed with PAD4 antibody. Quantitation of the soluble PAD4 band normalized to stain-free gels (b) was done using ImageJ software and data analyzed using GraphPad Prism software. Kruskal–Wallis test with Dunn's multiple comparisons of PAD4 abundance from uninjured sample compared to 7- and 16-day injured samples (c) revealed there were no significant changes at either time point, $H(2, N = 9) = 4.460$; $p = .1055$. The insoluble cytoskeletal-associated PAD4 levels (d) showed increased abundance. (e) Stain-free gels were used as protein loading controls for each fraction, respectively. (f) Quantitation of the cytoskeletal associated 75 kDa band revealed significant increased abundance at the 16-day post-injury time point, $H(2, N = 9) = 5.956$; $^*p = .0341$, but not at the 7-day injury time point ($p = .2021$). Data are presented as mean ± SD, $p < .05$ is considered significant.

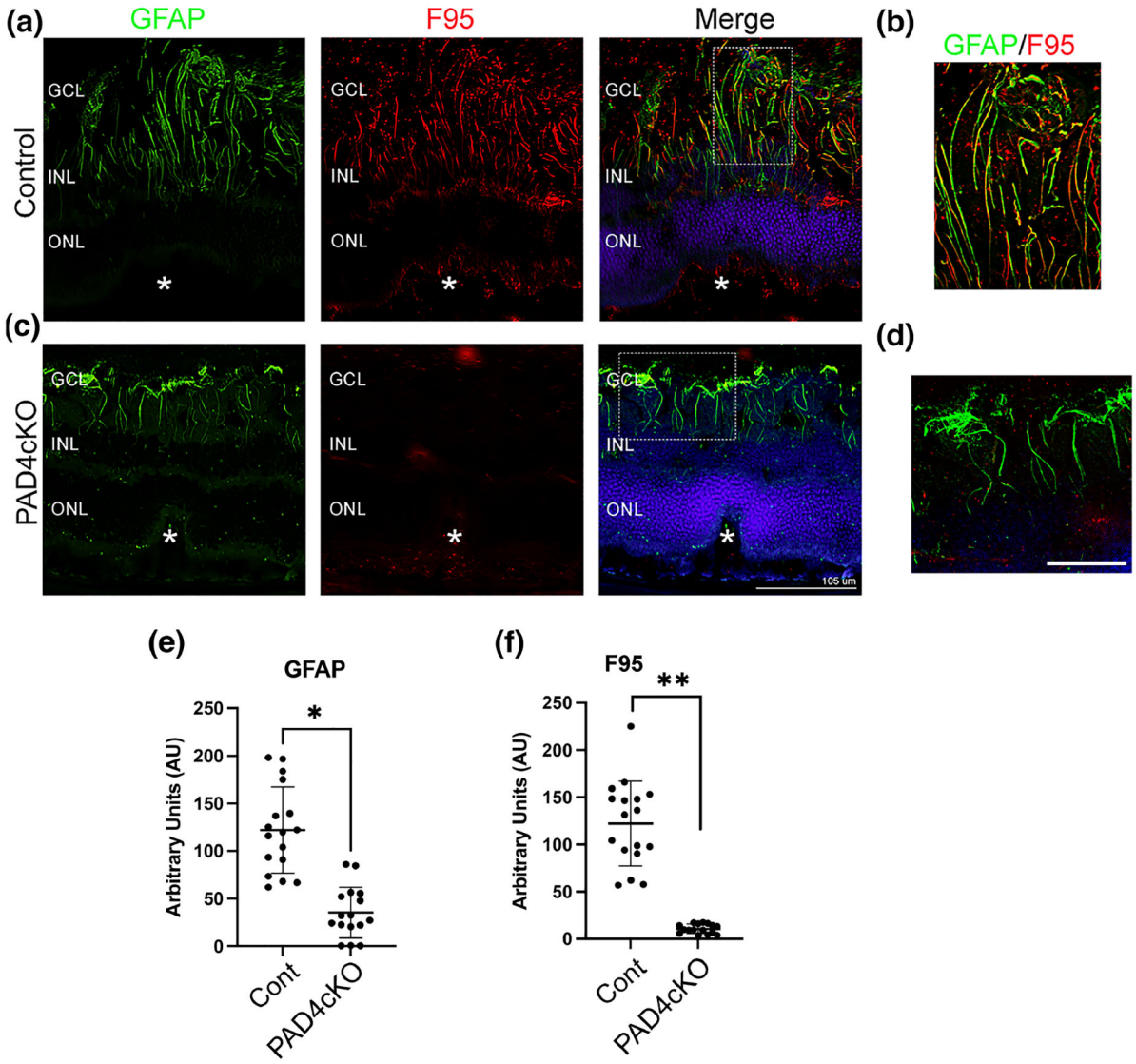

FIGURE 6.

Conditional knockout of PAD4 attenuates citrullination in mice subjected to retinal laser injury. Representative images from control (a) and PAD4cKO (c) retinas at 30 days post-laser injury. Cryosections were immunostained for GFAP (green) and citrullination with F95 (red). (a) F95 staining was evident on GFAP filaments in the lesions of control mice, while no F95 staining was observed in the lesions of PAD4cKO mouse retinas (c). Filamentous GFAP staining in PAD4cKO mouse retinas was reduced and sparse. (b,d) Enlarged images of the overlapping staining (Merge) boxed regions. The asterisks (a,c) denote the site of the laser lesion. GCL, ganglion cell layer; INL, inner nuclear layer, ONL, outer nuclear layer. Scale bar: a = 105 μm; scale bar: b = 35 μm. Quantification of GFAP (e) and F95 (f) staining using ImageJ software was performed (see File S3) and data analyzed using Mann–Whitney two-tailed nonparametric U test. Median GFAP staining of control samples and PAD4cKO samples were 120.0 and 29.75, respectively; the two groups were significantly different (U = 8, n_1 = 17, n_2 = 16, $^{**}p < .0001$). Median F95 staining of control samples and PAD4cKO

samples was 131.5 and 9.821, respectively; the two groups were also significantly different ($U = 0$, $n_1 = 17$, $n_2 = 16$, $^{**}p < .0001$). $N = 6$ mice/group, average of three sections per mouse. Data are presented as mean ± SD, $p < .05$ is considered significant.

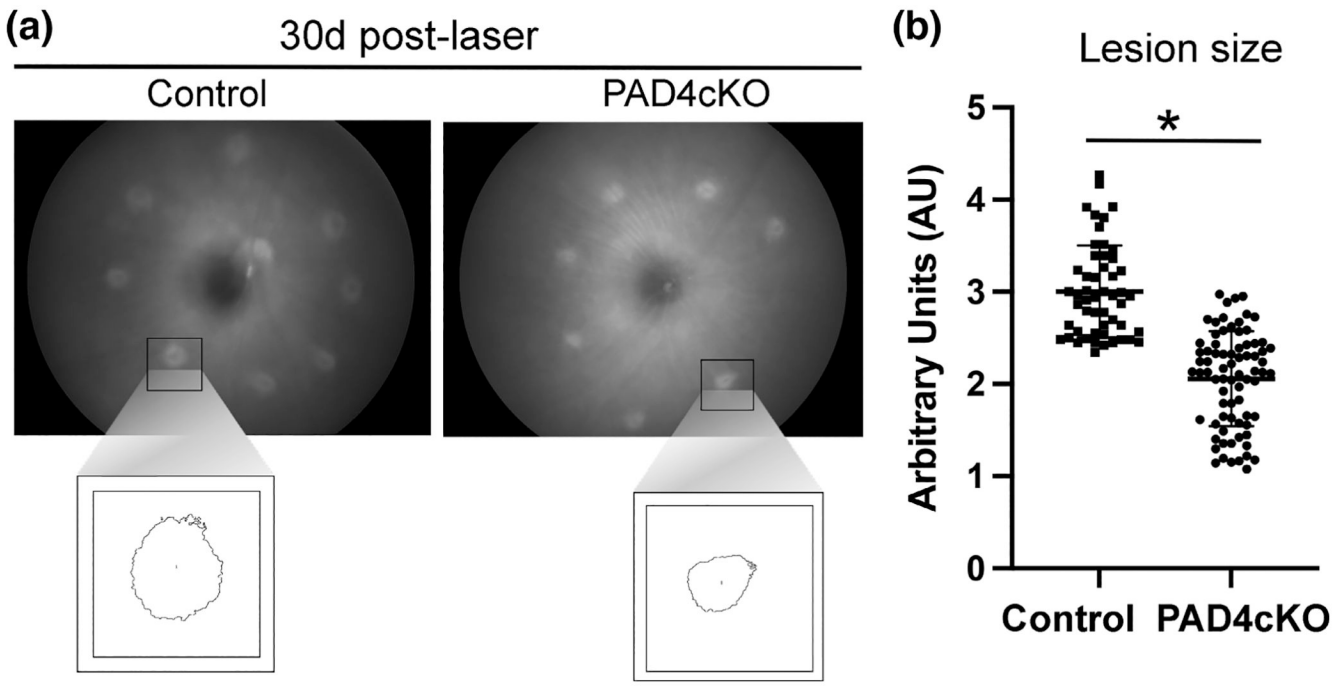

FIGURE 7.

Conditional knockout of PAD4 reduces lesion size of laser-damaged retinas. Retinal fundus images from control and PAD4cKO retinas from 30-day post-injured mice were acquired on a Phoenix Micron III fundus microscope. (a) Control mice revealed larger lesions compared to those from PAD4cKO mice. The boxed images represent measurements of individual lesions used for quantification. (b) Lesion sizes were quantified using ImageJ software and statistical analysis done using Mann–Whitney two-tailed nonparametric test. Median lesion size of control samples and PAD4cKO samples was 2.948 and 2.130, respectively; the two groups were significantly different ($U = 304.5$, $n_1 = 52$, $n_2 = 76$, $^{**}p < .0001$). $N = 7$ control mice (52 lesions) and $N = 10$ PAD4cKO mice (76 lesions) were analyzed. Data are presented as mean ± SD, $p < .05$ is considered significant.

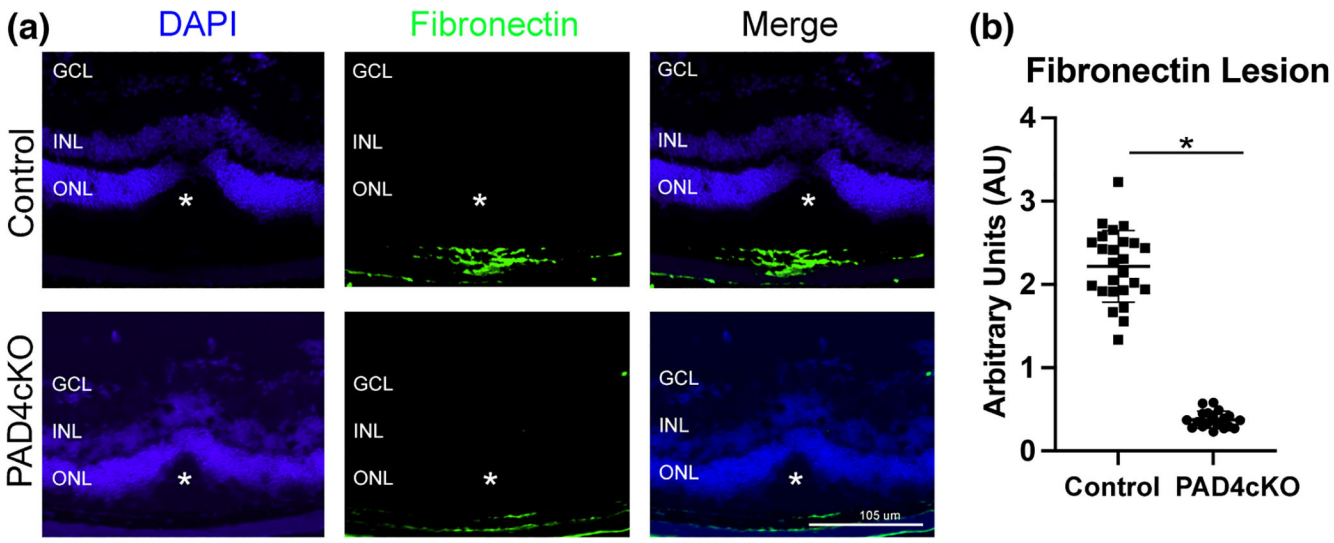

FIGURE 8.

Conditional knockout of PAD4 reduces fibronectin deposition in laser-injured retinas. Representative images of control and PAD4cKO retinas at 30-day post-injury from laser injured mice. (a) Images of control injured and PAD4cKO mice showing staining for fibronectin. Fibronectin deposition in the PAD4cKO lesion site was drastically reduced compared to the control. The asterisks (a) mark the position of laser lesion. (b) The area of staining representing fibronectin was quantified using ImageJ software (see also File S2). Statistical analysis using Welch's two-tailed parametric *t* test revealed significant differences between control (mean = 2.219 ± 0.4313) and PAD4cKO (mean = 0.3764 ± 0.1005) samples; $t_{27.36} = 20.63$, $*p < .0001$. $N = 6$ control mice (25 sections) and $N = 6$ PAD4cKO mice (19 sections) were analyzed. Data are presented as mean ± SD, $p < .05$ is considered significant. GCL, ganglion cell layer; INL, inner nuclear layer; ONL, outer nuclear layer.

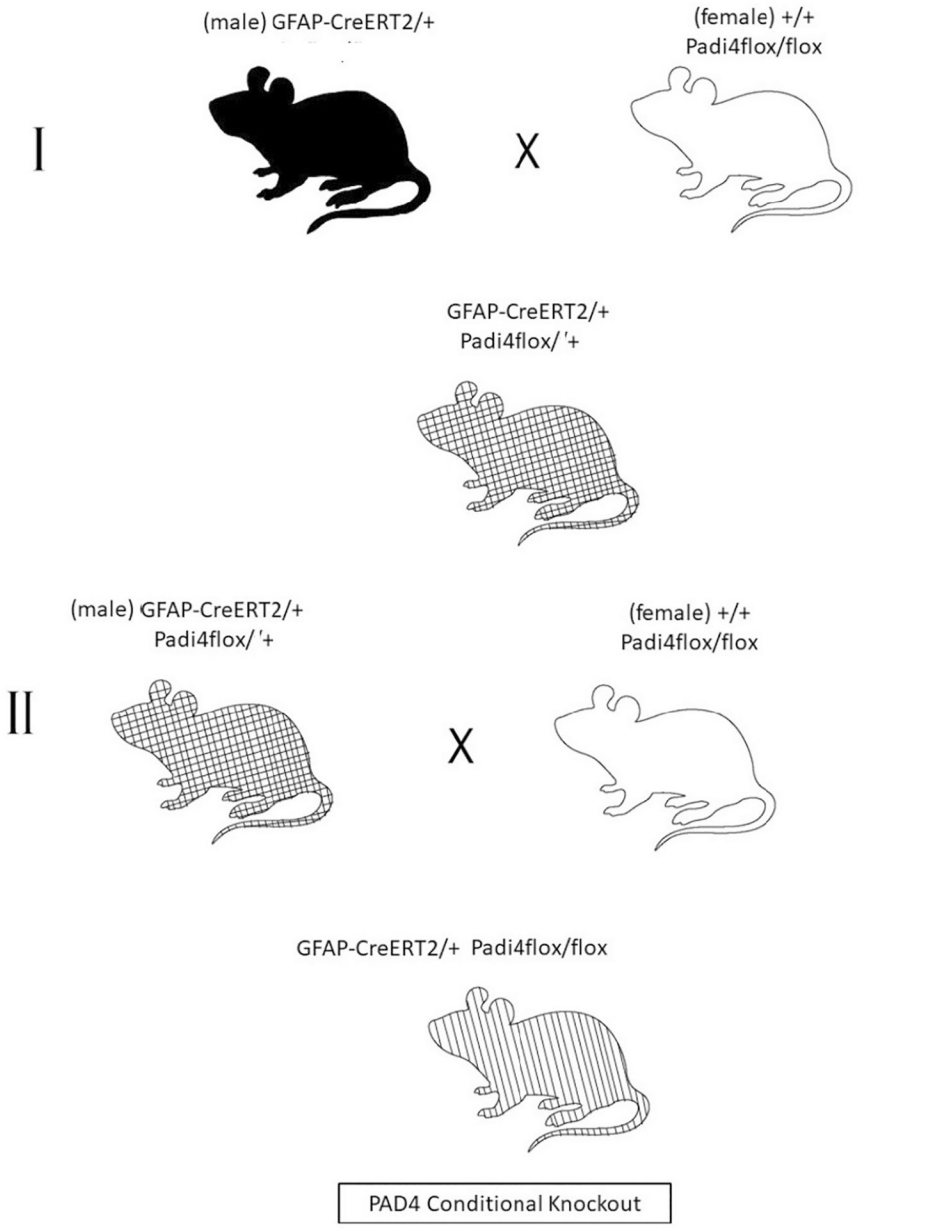

SCHEME 1.

Breeding strategy for PAD4 conditional knockout. The first crossing (I) consisted of a male GFAP-CreERT2/+ mouse and a female Padi4flox/flox mouse. The offspring from this mating, a heterozygous CreERT2/+ Padi4flox/+ line was selected and subsequently backcrossed with the homozygous +/+ Padi4flox/flox mouse line (II) to obtain the desired GFAP-CreERT2/+ Padi4flox/flox mouse line termed “PAD4cKO.” The +/+ Padi4flox/flox mice were used as “controls” and employed in experiments. Both groups were administered tamoxifen for all laser injury experiments.

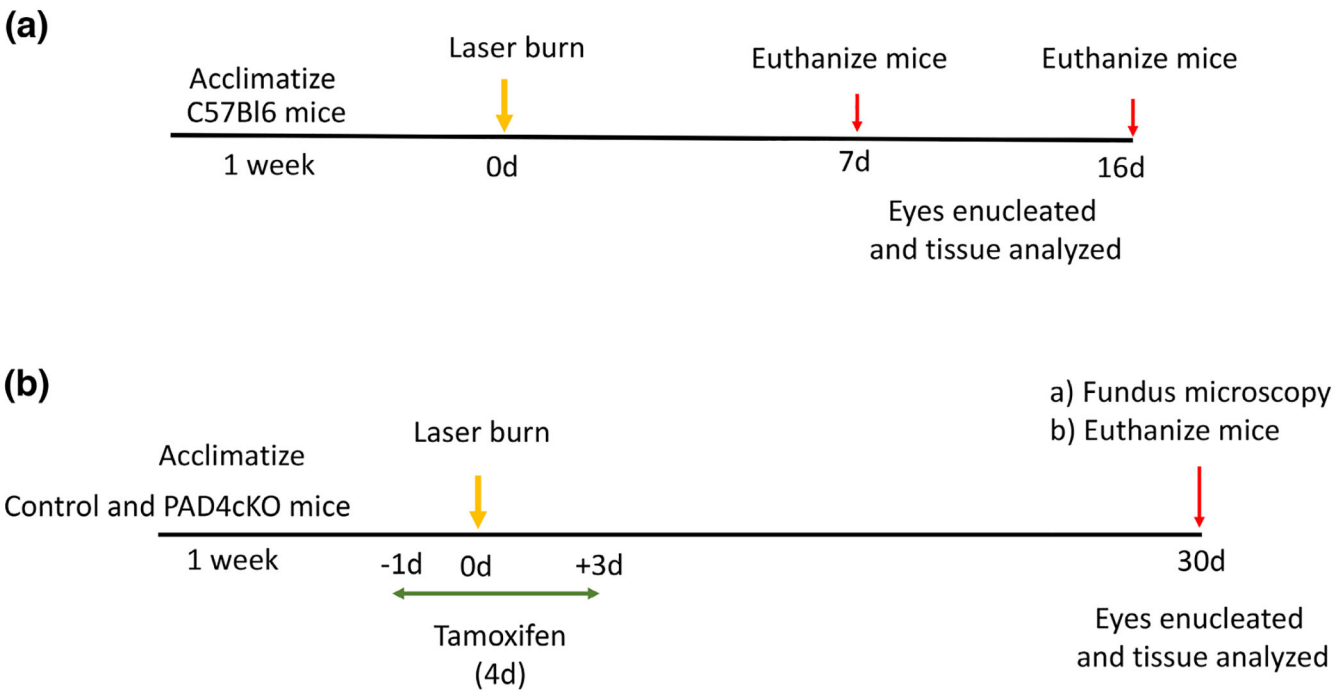

SCHEME 2.

Overview of experimental laser injury studies. (a) Wild-type C57Bl6 mice were subjected to laser injury and analyzed at 7- and 16-day post-injury for retinal gliosis. (b) Control and PAD4cKO mice were subjected to laser injury and analyzed at 30-day post-injury for subretinal fibrosis.

TABLE 1

Antibodies used for western blotting (WB) and immunofluorescence staining (IF).

Antibodies	Company/catalog number	RRIDs	Species	Dilution
Anti-GFAP	Abcam/4674	RRID:AB_304558	Chicken	IF: 1:500, 3 h @37°C
Anti-GFAP	Abcam/7779	RRID:AB_306067	Rabbit	WB: 1:4000, O/N @4°C
Anti-PAD4	Abcam/50247	RRID:AB_881875	Rabbit	IF: 1:100, 3 h @37°C
Anti-PAD4	Biolegend/684202	RRID:AB_2572090	Mouse	WB: 1:1000, O/N @4°C
Anti-citrullination (F95)	Millipore/MABN328	Monoclonal, IgM	Mouse	IF: 1:200; WB: 1:100, O/N @4°C
Anti-fibronectin	Abcam/199056	RRID:AB_2802127	Rabbit	IF: 1:100, O/N @4°C
Anti-rabbit HRP	Santa Cruz/Sc-2301	RRID:AB_650500	Goat	WB: 1:1000, 1 h @RT
Anti-mouse, Alexa 594	Thermofisher/11032	RRID:AB_2534091	Goat	IF: 1:500, 1 h @RT
Anti-chicken, Alexa 488	Thermofisher/32931	RRID:AB_2762843	Goat	IF: 1:500, 1 h @RT
Anti-rabbit, Alexa 647	Thermofisher/21245	RRID:AB_2535813	Goat	IF: 1:500, 1 h @RT
Anti-mouse, Alexa 594	Thermofisher/21044	RRID:AB_2535713	Goat	IF: 1:500, 1 h @RT
Anti-mouse, HRP	Santa Cruz/Sc-2302	RRID:AB_650499	Goat	WB: 1:1000, 1 h @RT
Anti-mouse, HRP	Jackson Immunoresearch/115-035-075	RRID:AB_2338508	Goat	WB: 1:1000, 1 h @RT